Supporting Information

Boosting Formaldehyde Oxidation at Low Temperature with Low-Loading Ag Catalyst via Surface Silanol Engineering of MCM-41

Yuchun Chang, [†a] Jing Xu, [†a] Yi Wang [a], Hui Wang* [a] and Zhenping Qu* [a]

[a] Key Laboratory of Industrial Ecology and Environmental Engineering (Ministry of Education, China), School of Environmental Science and Technology, Dalian University of Technology, Dalian, 116024, China

[†] These authors contributed equally to this work: Yuchun Chang, Jing Xu.

* Corresponding author: wanghui2017@dlut.edu.cn; quzhenping@dlut.edu.cn (Z.P. Qu)

1 Experimental Sections

1.1 Chemicals and materials

All chemicals were directly used after purchase without further purification: tetraethylorthosilicate (TEOS, AR, Sinopharm Chemical Reagent Co., Ltd.), hexadecyltrimethylammonium bromide ($[C_{16}H_{33}N(CH_3)_3]Br$, CTAB, AR, Sinopharm Chemical Reagent Co., Ltd.), sodium hydroxide (NaOH, AR, Sinopharm Chemical Reagent Co., Ltd.), nitric acid (HNO_3, 65-68%, Tianjin Kemiou Chemical Reagent Co., Ltd.), silver nitrate ($AgNO_3$, AR, Tianjin Kemiou Chemical Reagent Co., Ltd.), trioxymethylene (AR, Acros Organics).

1.2 Synthesis of MCM-41

MCM-41 was synthesized by using a typical procedure reported by Stucky et al [1]. In this synthesis, CTAB was first dissolved into 2M NaOH aqueous solution, then by adding TEOS, the mixture was stirred vigorously for 2 h. The resulting suspension was transferred into a Teflon-lined stainless-steal (SS) autoclave for crystallization at 100 °C for 3 days. The precipitate was repeatedly filtered with deionized (DI) water until neutral, then dried overnight at 80 °C and calcined in air at 550 °C for 6 h with a heating rate of 0.75 °C /min. The obtained white powder was donated as MCM-41.

1.3 Synthesis of acid-treated MCM-41

The acid-treated MCM-41 support was synthesized by dispersing 1g MCM-41 into nitric acid solution with different concentrations (0.38, 0.57 and 0.76 M). After constantly stirred at 60 °C for 2 h, the mixture was washed for several times with DI water until neutral and then dried at 80 °C overnight. The post-treated samples were collectively donated as MCM-41-X, (X: 0.38, 0.57 and 0.76).

1.4 Synthesis of Ag/MCM-41 and Ag/MCM-41-X

Conventional incipient wetness impregnation was used to prepare Ag based samples. Typically, a certain amount of $AgNO_3$ was dissolved in DI water, in which the supports (MCM-41, MCM-41-0.38, MCM-41-0.57 and MCM-41-0.76) were added. The slurry was stirred for 3 h, aged at room temperature for 24 h, and then dried overnight at 80 °C. Before reaction, all samples were calcinated in 20% O_2-Ar at 600 °C for 2 h, and then heated in 10% H_2-Ar 500 °C for 1 h to be activated. The obtained samples were named as Ag/MCM-41 and Ag/MCM-41-X, (X: 0.38, 0.57 and 0.76). Inductively coupled plasma-optical emission spectrometry (ICP-OES) results revealed that the actual loading of Ag species on the catalysts was approximately 0.95-1.0 wt.% (**Table S1)**.

2 Catalyst characterization

X-ray diffraction (XRD) was measured on a Rigaku powder diffractometer equipped with a Cu Kα radiation source (λ = 1.542 Å), operated at 40 kV and 40 mA. The N_2 absorption/desorption processes at -196 °C were carried out with an automatic physical adsorption Instrument (Quantachrome, S1-9, America). The surface area and micropore volume (V_{micro}) were calculated using the Brunauer-Emmett-Teller (BET) and t-plot methodology, respectively. Mesopore volume (V_{meso}) and pore size distribution were evaluated by BJH model. Transmission electron microscopy (TEM) images were performed on a Tecnai G^2 20S-Twin. Inductively coupled plasma-optical emission spectrometry (ICP-OES, OPTIMA 2000DV) was use to get the actual content of silver in the catalysts. The Ultraviolet–Visible diffuse reflectance spectra (UV-Vis DRS) were collected on a SHIMADZU UV-2600 in the range of 190-800 nm. Raman spectrum was recorded on a Renishaw PLC inVia Qontor spectrometer with the excitation wavelength of 532 nm. Fourier Transform infrared spectroscopy (FTIR) was measured on a Thermos Nicolet IS 10. X-ray photoelectron spectroscopy (XPS) was

implemented on a ESCALAB 250 (Thermo VG) equipped with a monochromatic X-ray source of Al Kα (1486.6 eV) under ultra-high vacuum.

^{29}Si cross-polarization Magic Angle Spinning Nuclear Magnetic Resonance (^{29}Si CP/MAS NMR) experiments were performed with a contact time of 4 ms, a recycle delay of 4 s and a spinning rate of 6 kHz on an Agilent DD2-500 MHz spectrometer. ^{1}H Magic Angle Spinning Nuclear Magnetic Resonance (^{1}H MAS NMR) spectra were recorded on a 4 mm probe with a spinning rate at 10 kHz on an Agilent DD2-500 MHz spectrometer. Prior to the experiments, all samples were dehydrated at 300 °C under vacuum for 12 h. All of the spectra were normalized based on the mass of samples. Temperature-programmed desorption of ammonia (NH_3-TPD) was measured on an *in situ* mass spectrometer (Pfeiffer vacuum OmniStar GSD320).

In situ diffuse reflection infrared Fourier transform spectroscopy (DRIFTS) was recorded in a Thermos Nicolet IS10 by using variable-temperature quartz cells. All spectra were recorded with a resolution of 4 cm^{-1} and accumulating 32 scans. Prior to analysis, the samples were treated in a 30 mL/min He flow at 300 °C for 30 min to eliminate the interference of the adsorbed water. Background spectra were recorded at 30, 50, 70 and 80 °C from 4000 to 1000 cm^{-1}, respectively. Subsequently, HCHO was adsorbed at 30 °C for 30 min, followed by purging with He for 30 min at the same temperature. Then, 20 vol% O_2/He was introduced, and the temperature was increased stepwise from 30 to 80 °C. At each target temperature, the reaction was allowed to proceed for 30 min, and the spectrum was recorded at the end of this period.

3 Catalytic tests

The catalyst (180 mg, 20-40 mesh) was placed in a continuous flow fixed-bed quartz reactor, with an inner diameter of 8 mm. For the catalyst testing, 100 ppm HCHO was introduced in 60 mL/min 20 vol% O_2/Ar, giving a gas hourly space velocity

(GHSV) of 20,000 mL/g·h^{-1}. The HCHO conversion was calculated based on the flowing equation:

$$HCHO\ conversion\ (\%) = \left(1 - \frac{[CO_2]_{out}}{[HCHO]_{in}}\right) \times 100,$$

where $[HCHO]_{in}$ and $[CO_2]_{out}$ are the inlet HCHO concentration and the outlet CO_2 concentration, respectively.

The turnover frequency (TOF) was interpreted as the amount of converted HCHO molecular on the surface of an Ag atom in a second. It could be calculated as follows:

$$TOF_{Ag} = \frac{C_{HCHO} X_{HCHO} V_{gas} M_{Ag}}{m_{cat} w_{Ag} D_{Ag}} [s^{-1}],$$

where C_{HCHO} (ppm) is the concentration of HCHO in the gas flow, X_{HCHO} is the HCHO conversion to CO_2 (%), V_{gas} represents the molar flow rate of the reactants; M_{Ag} is the relative atomic mass (g·mol^{-1}); m_{act} is the mass of catalysts used in the fixed reactor (g); w_{Ag} is the Ag content measured by ICP-OES (%); D_{Ag} represents the dispersion of Ag atoms calculated by the average particle size from TEM images.

The reaction rate (r, mol·g^{-1}·s^{-1}) was calculated according to the equation below:

$$r = \frac{F \times X}{w_{Ag}},$$

where F is the gas velocity (mol·s^{-1}), X is the HCHO conversion (below 15%), w_{Ag} is the mass of Ag (g).

Activation energy (E_a) was calculated according to Arrhenius equation:

$$r = Ae^{\left(-\frac{E_a}{RT}\right)},$$

where R is the ideal gas constant (8.314 J·mol^{-1}·K^{-1}), T is the actual reaction temperature (K) and A is a constant.

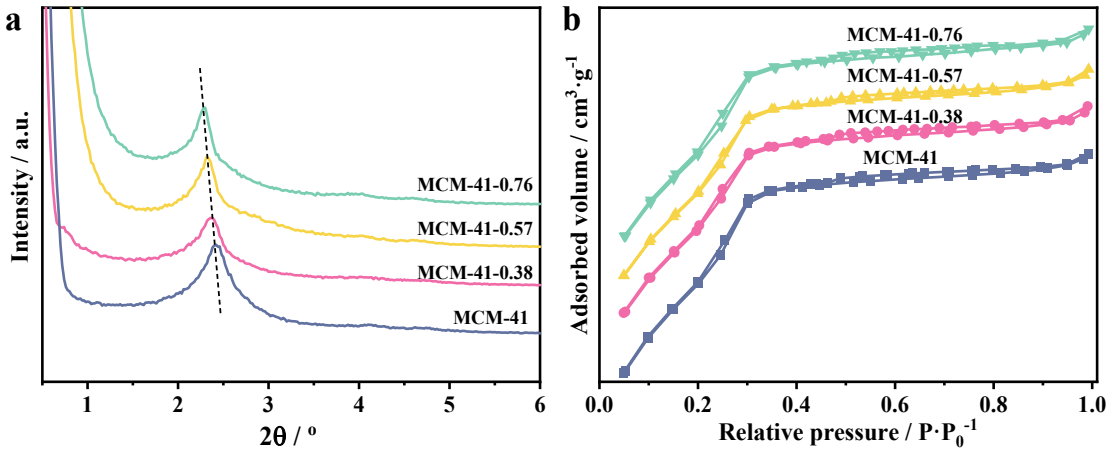

Fig. S1. Physical structure of MCM-41, MCM-41-0.38, MCM-41-0.57 and MCM-41-0.76 supports. (a) small-angle X-ray diffraction (SAXD) patterns; (b) nitrogen adsorption-desorption isotherms.

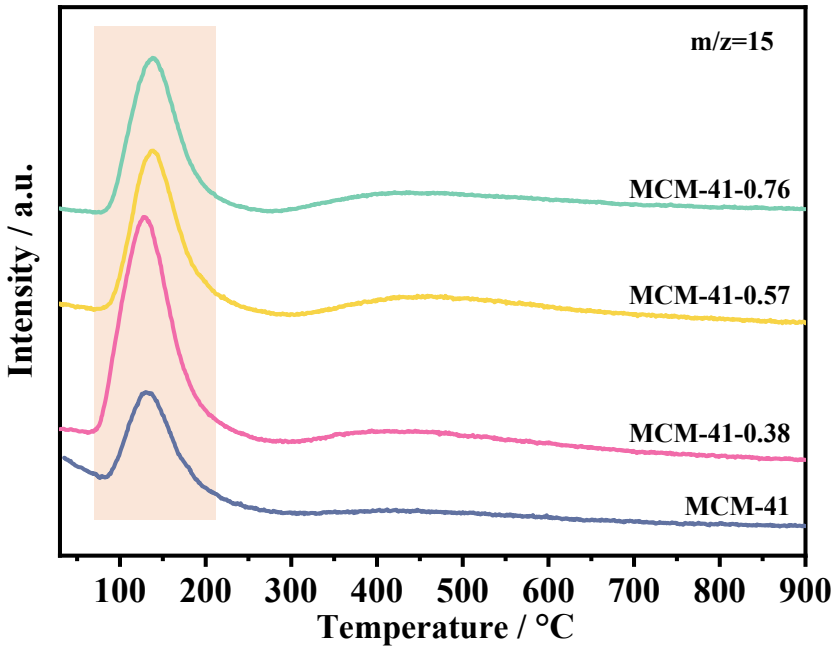

Fig. S2. NH_3-TPD profiles of MCM-41, MCM-41-0.38, MCM-41-0.57 and MCM-41-0.76 samples.

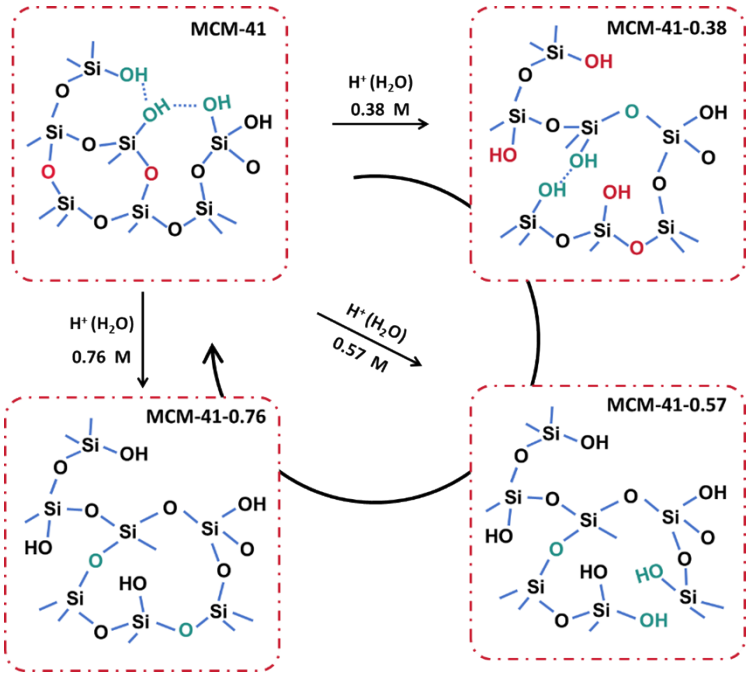

Fig. S3. Schematic diagram of variation of silanol groups during acid pretreatment.

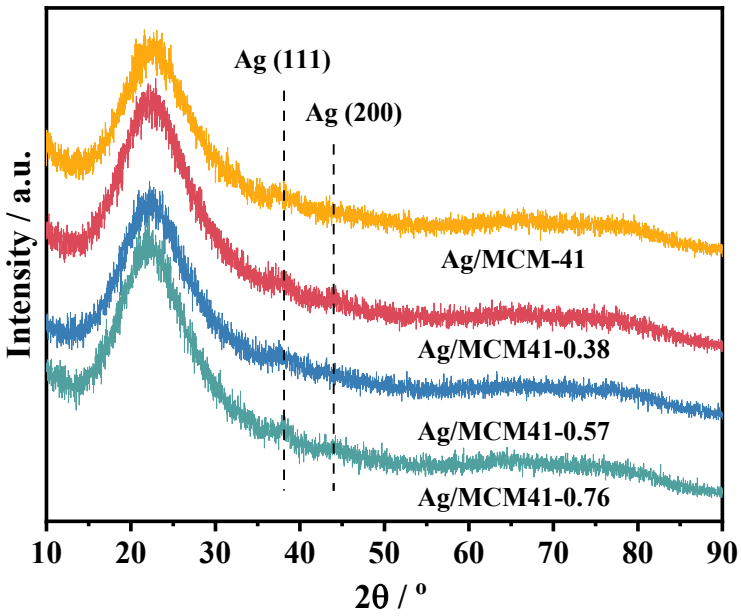

Fig. S4. Wide-angle XRD patterns of Ag/MCM-41, Ag/MCM-41-0.38, Ag/MCM-41-0.57 and Ag/MCM-41-0.76.

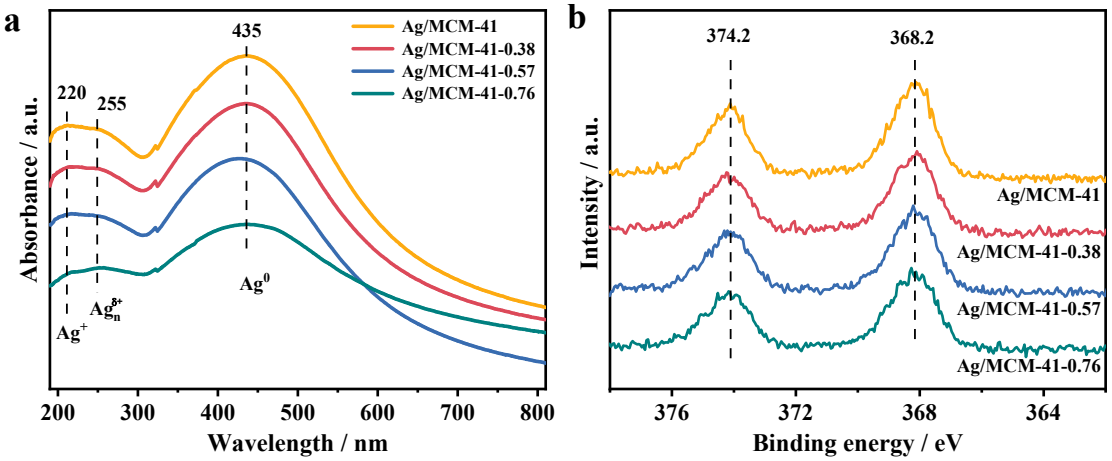

Fig. S5. Coordination status of Ag species on Ag/MCM-41, Ag/MCM-41-0.38, Ag/MCM-41-0.57 and Ag/MCM-41-0.76: (a) UV-Vis DRS; (b) Ag 3d XPS.

The chemical state of Ag for different samples pretreated with H_2 reduction at 500 °C was investigated by UV-Vis DRS and Ag 3d XPS spectra. The four samples exhibit three similar absorption bands at around 220, 255 and 435 nm. The weak bands at 220 and 255 nm are ascribed to the $4d^{10}$-$4d^9 5s^1$ transition of isolated Ag^+ ion and Ag clusters ($Ag_n^{\delta+}$), respectively. While the strong broad absorption band centered at 435 nm is assigned to metallic Ag NPs [2], and the dominate state of Ag is metallic Ag^0. Additionally, Ag 3d XPS spectra exhibit two peaks at 368.2 eV (Ag $3d_{5/2}$) and 374.2 eV (Ag $3d_{3/2}$) for all the four catalysts, corresponding to metallic Ag species [3], and no significant shifts is observed among the four samples.

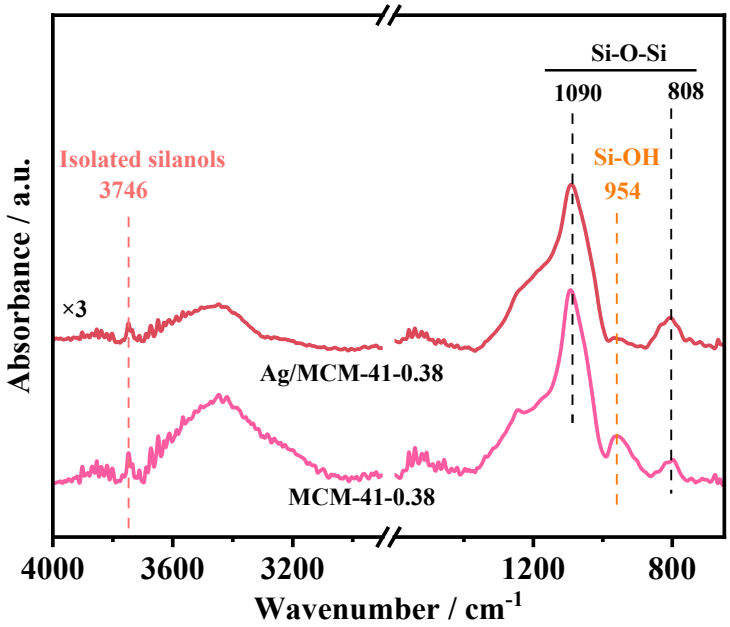

Fig. S6. FTIR spectra of MCM-41-0.38 and Ag/MCM-41-0.38.

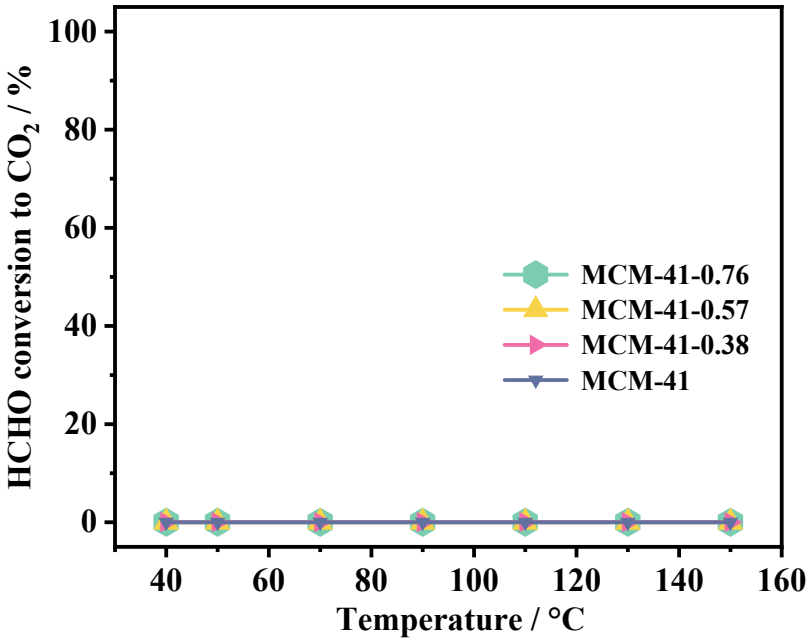

Fig. S7. HCHO oxidation performance on MCM-41 and MCM-41-X supports.

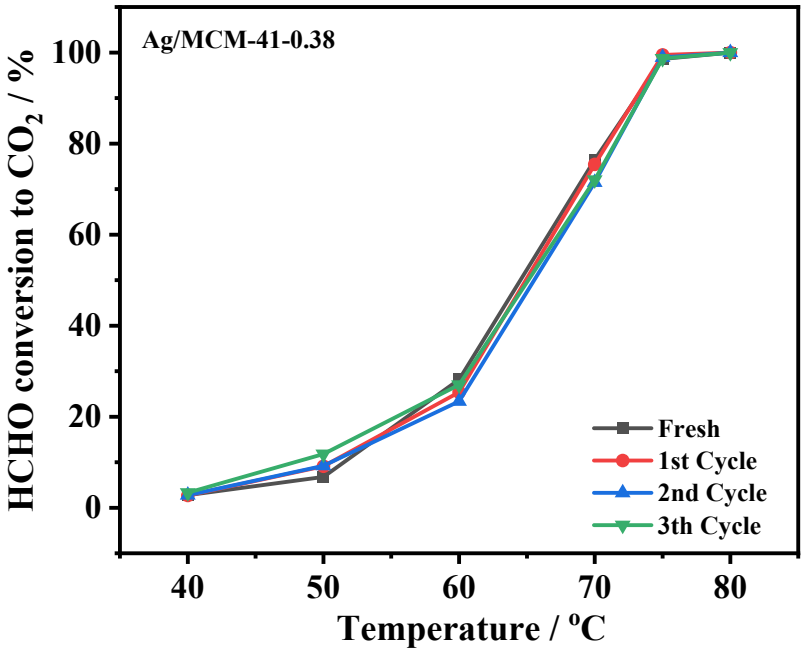

Fig. S8. Cyclic stability test of Ag/MCM-41-0.38.

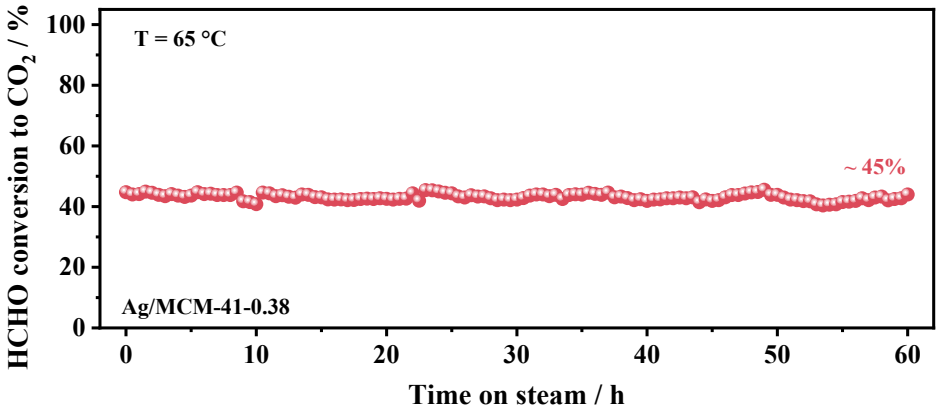

Fig. S9. Stability of Ag/MCM-41-0.38 at 65 °C.

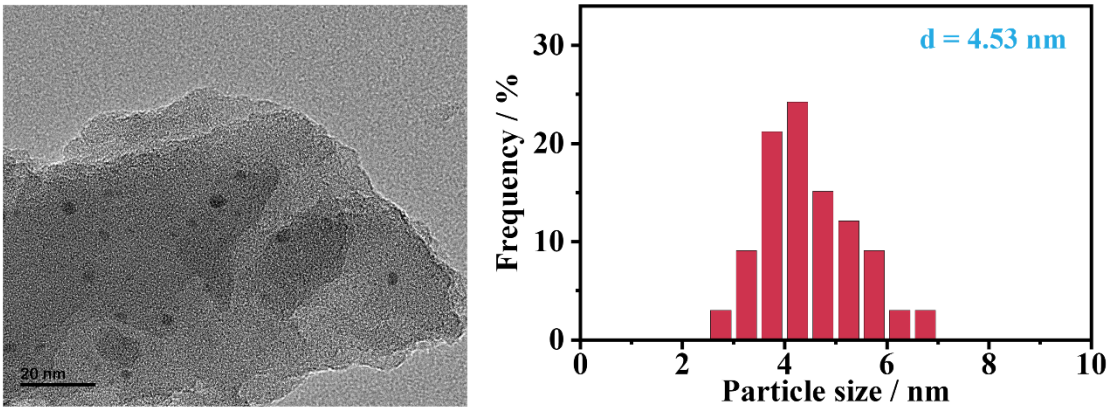

Fig. S10. TEM image and particle size distribution of Ag/MCM-41-0.38 after cyclic test.

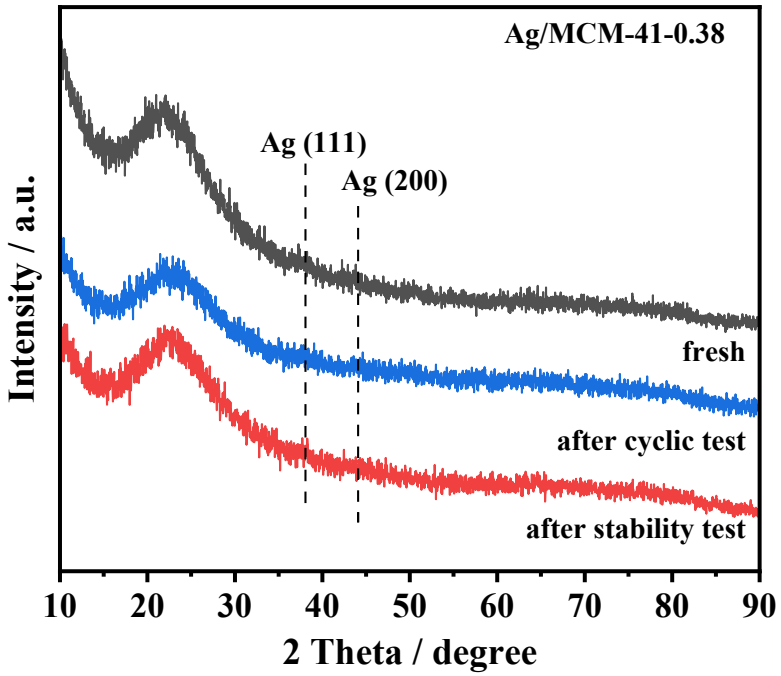

Fig. S11. XRD patterns of Ag/MCM-41-0.38 before and after cyclic test and stability test.

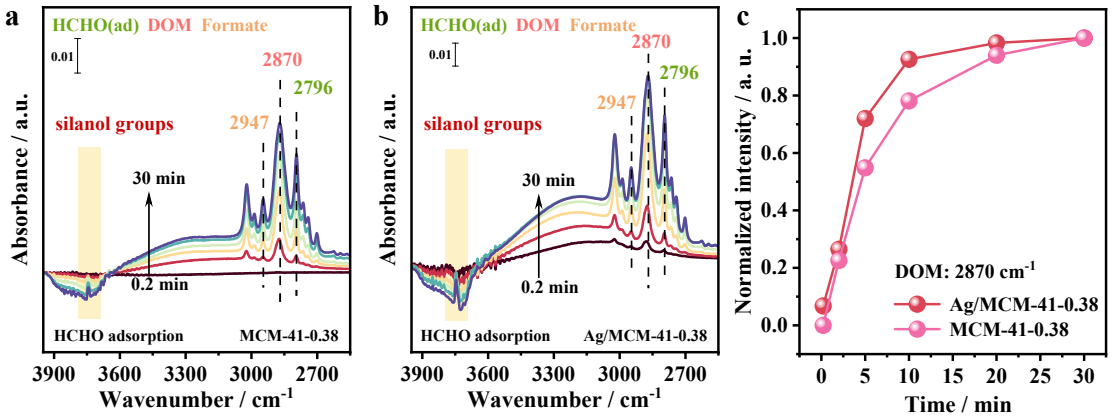

Fig. S12. HCHO adsorption process over MCM-41-0.38 and Ag/MCM-41-0.38 catalysts. (a-b) *in situ* DRIFT spectra of HCHO adsorption; (c) dynamic changes of normalized intensity of DOM (2870 cm^{-1}) with the increase of adsorption time in a flow of HCHO/He.

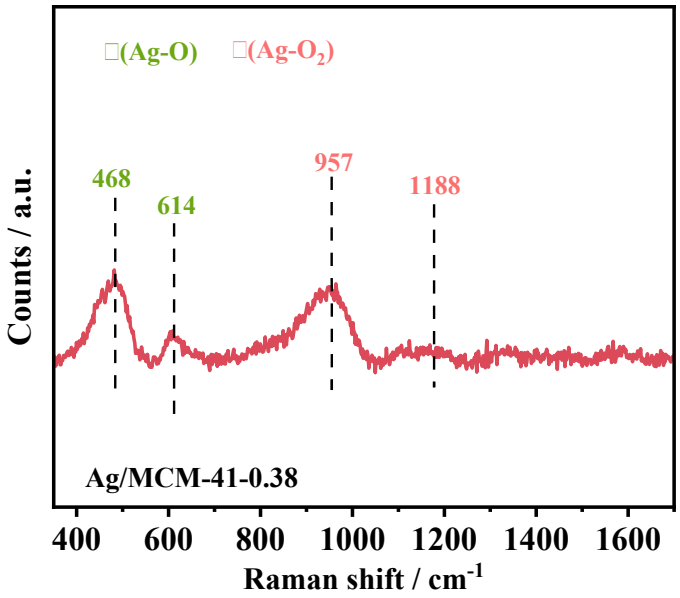

Fig. S13. Raman spectrum of Ag/MCM-41-0.38.

Raman spectrum was used to observe the existence of oxygen species on Ag/MCM-41-0.38. Bands at 468 and 614 cm^{-1} are assigned to surface atomic oxygen species which are weakly chemisorbed on Ag surfaces, and subsurface atomic oxygen, respectively [4]. The bands at 957 and 1188 cm^{-1} are attributed to chemisorbed molecular oxygen species[5]. This indicates that Ag/MCM-41-0.38 catalyst can activate and dissociate O_2 molecule to active O species, which will be conductive to the degradation of intermediate species (**Fig. 4b**).

Table S1. Content of Ag in Ag/MCM-41, Ag/MCM-41-0.38, Ag/MCM-41-0.57 and Ag/MCM-41-0.76.

Samples	Content of Ag* (wt.%)
Ag/MCM-41	1.10
Ag/MCM-41-0.38	0.95
Ag/MCM-41-0.57	1.15
Ag/MCM-41-0.76	1.00

* Determined by ICP-OES.

Table S2. Textural parameters of MCM-41, MCM-41-0.38, MCM-41-0.57 and MCM-41-0.76.

Samples	BET surface area ($m^2 \cdot g^{-1}$)	Pore volume ($cm^3 \cdot g^{-1}$)	D_{pore} (nm)	Lattice spacings of (100) d_{100} (nm)
MCM-41	878.7	0.52	2.37	3.7
MCM-41-0.38	875.4	0.51	2.34	3.8
MCM-41-0.57	861.7	0.51	2.36	3.9
MCM-41-0.76	867.9	0.51	2.37	3.9

Table S3. Relative content proportions (%) in the ^{29}Si CP/MAS NMR and ^{1}H MAS NMR over MCM-41, MCM-41-0.38, MCM-41-0.57 and MCM-41-0.76.

Samples	Relative content proportions (%)						
	^{29}Si NMR resonance*			^{1}H NMR resonance**			
	Q^2	Q^3	Q^4	δ=1.9 ppm	δ=2.5 ppm	δ=3.1 ppm	δ=3.9 ppm
	$[(SiO)_2{-}Si(OH)_2]$	$[(SiO)_3{-}Si(OH)]$	$[(SiO)_4{-}Si]$	Isolated silanol groups	Weak H-bonded silanol groups	Medium H-bonded silanol groups	Strong H-bonded silanol groups
MCM-41	13.1	61.0	26.0	67.5	20.5	5.7	6.3
MCM-41-0.38	7.6	74.9	17.5	69.2	19.3	11.5	0
MCM-41-0.57	10.0	68.3	21.7	73.7	12.4	14.0	0
MCM-41-0.76	11.5	61.9	26.6	70.9	13.6	15.1	0

*: Obtained from ^{29}Si CP/MAS NMR resonance spectra.

**: Obtained from ^{1}H MAS NMR resonance spectra.

Table S4. $(Q^2+Q^3)/Q^4$, I(Si-OH)/I(Si-O-Si) and NH_3 desorption peak areas over MCM-41, MCM-41-0.38, MCM-41-0.57 and MCM-41-0.76.

Samples	$(Q^2+Q^3)/Q^4$ (a.u.)	I(Si-OH)/I(Si-O-Si) (a.u.)	NH_3 desorption peak areas (1E-9)
MCM-41	2.84	0.08	2.30
MCM-41-0.38	4.71	0.25	5.90
MCM-41-0.57	3.61	0.20	4.01
MCM-41-0.76	2.76	0.21	4.00

Table S5. Performance of Ag/MCM-41-0.38 compared to other silver-based catalysts for oxidation of HCHO.

Catalysts	Initial HCHO concentration (ppm)	GHSV ($mL \cdot g^{-1} \cdot h^{-1}$)	T_{100} (°C)	Ag content (wt.%)	Ref.
2K-Ag/Al_2O_3	110	100,000	65	7.77	[2]
3D 1.7%K-Ag/Co_3O_4	100	30,000	70	6.4	[6]
3D Ag/Co_3O_4	100	30,000	100	8.2	[6]
Ag/rCeO_2	810	84,000	96 (T_{90})	4.81	[7]
Ag/TiO_2-A	130	100,000	125	8.0	[8]
Ag/γ-Al_2O_3	200	9,000	85	10.3	[9]
Ag/CeO_2-rod	220	36,000	80	4.87	[10]
Ag/AlOOH(c)	180	18,000	75	4	[11]
5CTs-10Ag/HP-Sep-300	100	6000	52	10	[12]
Ag/Fe0.1-MnOx	400	30,000	90	2.88	[13]
Ag-HMO	400	30,000	110	9.7	[14]
Ag_1/HMO	140	92,000	130	15.5	[15]
Ag/SBA-15	100	36,000	150	10	[16]
Ag/Al_2O_3	130	100,000	80	8	[17]
Ag/TiO_2	130	100,000	170	8	[17]
Ag/Mn-CO	300	75,000	100 (T_{90})	6.6	[18]
Ag/Al-600H_2	100	100,000	125	1	[19]
Ag/MCM-41-0.38	100	20,000	75	1	This work

Reference

1. Q. S. Huo, D. I. Margolese and G. D. Stucky, *Chem Mater*, 1996, **8**, 1147-1160.
2. X. Chen, M. Chen, G. He, F. Wang, G. Xu, Y. Li, C. Zhang and H. He, *The Journal of Physical Chemistry C*, 2018, **122**, 27331-27339.
3. Y. Ji, X. Chen, S. Liu, S. Song, W. Xu, R. Jiang, W. Chen, H. Li, T. Zhu, Z. Li, Z. Zhong, D. Wang, G. Xu and F. Su, *ACS Catalysis*, 2023, **13**, 1230-1239.
4. Z. Zhao and M. A. Carpenter, *The Journal of Physical Chemistry C*, 2013, **117**, 11124-11132.
5. L. Ren, W. Dai, X. Yang, Y. Cao, Z. Xie and K. Fan, *Chinese Journal of Catalysis*, 2006, **27**, 115-118.
6. B. Bai and J. Li, *ACS Catalysis*, 2014, **4**, 2753-2762.
7. L. Yu, R. Peng, L. Chen, M. Fu, J. Wu and D. Ye, *Chemical Engineering Journal*, 2018, **334**, 2480-2487.
8. X. Chen, H. Wang, M. Chen, X. Qin, H. He and C. Zhang, *Applied Catalysis B: Environmental*, 2021, **282**.
9. Y. Wang, Z. Qu, J. Xu and B. Huang, *Applied Catalysis A: General*, 2020, **602**.
10. G. Jiang, Y. Su, H. Li, Y. Chen, S. Li, Y. Bu and Z. Zhang, *Applied Surface Science*, 2021, **549**.
11. Y. Wang, B. Huang, J. Xu, N. Li and Z. Qu, *Catalysis Letters*, 2021, **151**, 2376-2383.
12. D. Li, P. Liu, Y. Zheng, Y. Wu, L. Ling, L. Chen, F. Hao, Y. Lv, W. Xiong and H. a. Luo, *Journal of Environmental Chemical Engineering*, 2022, **10**.
13. D. Li, G. Yang, P. Li, J. Wang and P. Zhang, *Catalysis Today*, 2016, **277**, 257-265.
14. Z. Huang, X. Gu, Q. Cao, P. Hu, J. Hao, J. Li and X. Tang, *Angewandte Chemie International Edition*, 2012, **51**, 4198-4203.
15. Y. Chen, J. Gao, Z. Huang, M. Zhou, J. Chen, C. Li, Z. Ma, J. Chen and X. Tang, *Environmental Science & Technology*, 2017, **51**, 7084-7090.
16. N. Li, B. Huang, X. Dong, J. Luo, Y. Wang, H. Wang, D. Miao, Y. Pan, F. Jiao, J. Xiao and Z. Qu, *Nature Communications*, 2022, **13**.
17. X. Chen, H. Deng, M. Chen, X. Qin, L. Wang and C. Zhang, *Chemical Engineering Journal*, 2026, **533**.
18. S. Hu, J. Zhang, X. Chen, X. Qin, J. Yao and C. Zhang, *Journal of Environmental Sciences*, 2024, **138**, 709-718.
19. X. Chen, S. Hu, X. Qin, M. Chen, J. Zhang, X. Bao and C. Zhang, *ACS Applied Nano Materials*, 2023, **6**, 8763-8771.